in Fig. 2. A positive-going periodic ramp voltage varies linearly with time between the breakdown voltage of about −7 V and a small positive value (+0·8 V). The luminescence is periodically modulated according to eqn. 1 and exhibits the essentially exponential time dependence. The 3 dB cutoff frequency of the lowpass filter connected to the postamplifier was 10 kHz in this case.

Fig. 3 demonstrates the feasibility of fast p.l. pulse modulation. Pulses of positive polarity on a negative offset voltage (pulse-repetition rate of 1 Mbit/s) modulate the luminescence intensity according to the bit pattern 1100. The pulse response of the luminescence signal (Fig. 3) exhibits considerable roundings because 1 MHz is beyond the 3 dB frequency response of the available preamplifier. Using a broadband preamplifier, however, it should be possible to modulate the luminescence up to several megahertz, preserving a sufficient signal/noise ratio. Further raising of the luminescence intensity and further improvement of the experimental equipment by, for example, the use of antireflection coating, optimisation of the metal transparency, higher quantum efficiency of the crystal and of the cathode, and higher illumination intensity should allow the operation to be extended to higher frequencies.

Conclusions: The main features of this new concept of luminescence modulation are:

(*a*) Simple preparation of semitransparent Schottky-barrier diode with small contact diameter corresponding to the focus area of the laser beam.

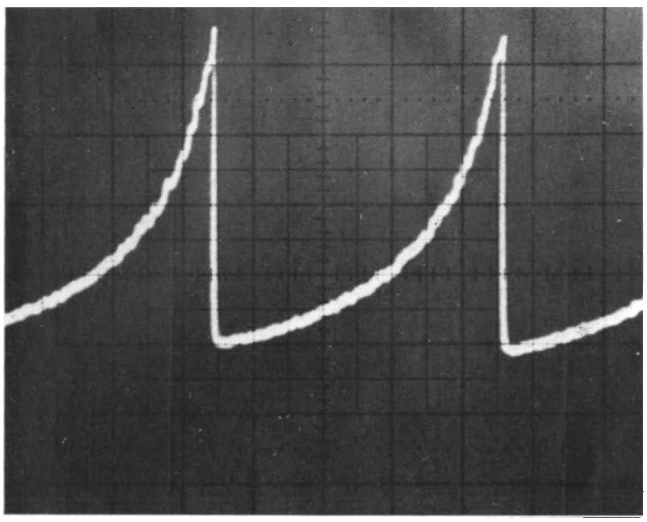

Fig. 2 *Characteristic variation of p.l. intensity with periodic positive-going ramp voltage varying between breakdown voltage and +0·8 V*
Vertical: 2 V/division, horizontal: 1 ms/division

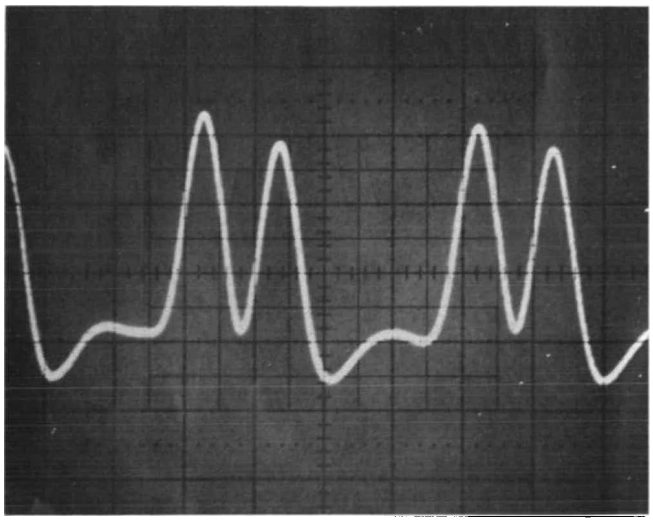

Fig. 3 *Pulse-modulated p.l. intensity*
1 Mbit/s, bit pattern 1100
Vertical: 5 V/division, horizontal: 1 μs/division

(*b*) Compatibility with integrated semiconductor circuits.

(*c*) Fast response of p.l. signal to applied voltage pulses (obtainable minimum risetimes and falltimes presumably determined by the minority-carrier lifetimes) and applicability to optical signal transmission.

(*d*) Operation both in a photodiode and modulated-luminescence mode.

(*e*) Hence favourable for applications requiring pure optical broadband information transfer with random laser-beam access.

A possible application—in connection with standard laser-beam deflection[3]—is thought to be in the field of beam-accessed data memories with optical readout of binary information from a 2-dimensional array of Schottky-barrier diodes (by voltage-controlled luminescence operation) and perhaps with optical data recording (by photodiode operation in connection with transistor flip–flops). Further applications might be within the framework of optical communication techniques[4] and integrated optical circuits.

Acknowledgment: The author wishes to thank Prof. B. G. Bosch for his support.

U. LANGMANN

Institut für Elektronik
Ruhr-Universität Bochum
D-4630 Bochum, Postfach 2148, W. Germany

3rd September 1975

References

1 HETRIC, R. E., and YOUNG, K. F.: 'Effect of surface electric fields on radiative recombination in CdS', *J. Appl. Phys.*, 1971, **42**, pp. 2882–2885
2 LANGMANN, U.: 'Photoluminescence of *n*-GaAs at transparent Schottky contacts', *Appl. Phys.*, 1973, **1**, pp. 219–221.
3 PEPPERL, R.: 'Die digitale Laserstrahlablenkung und ihre Anwendungen', *Phys. Bl.*, 1973, **29**, pp. 352–361.
4 HILL, B.: 'Verknüpfung von Nachrichtenkanälen mit digitalen Lichtablenkern', *Nachrichtentech. Z.*, 1970, **23**, pp. 549–552.

NUMERICAL CHECK OF G.T.D. NEAR-FIELD CALCULATIONS FOR THE METEOSAT SATELLITE

Indexing terms: Antenna radiation patterns, Microwave antennas, Satellite links

The near-field and the far-field patterns from the high-gain S band antenna on the METEOSAT are calculated by the geometrical theory of diffraction. The far field is transformed into the near field through an expansion in spherical harmonics. The resulting transformed field agrees well with the g.t.d. near field.

The first European meteorological satellite, METEOSAT, is currently being developed by ESTEC. It will be equipped with a directive, electronically despun antenna (e.d.a.). Owing to the rotation of the spin-stabilised satellite, it is necessary that the beam rotates in the opposite direction to point towards the Earth. The geometry of METEOSAT is indicated in Fig. 1. The e.d.a.[1] consists of 32 columns, each with four horizontally polarised halfwave dipoles placed around a 32-faceted cylinder above the circularly cylindrical main satellite structure. The beam is formed by four or five columns. The power is gradually shifted from column to column to excite the columns which, at a given instance, point towards the Earth.

The important antenna parameter is the directivity in the coverage region which extends about 9° off the geocentric direction. However, in the clean rooms to be used during the integration and the testing of the satellite, it will not be possible to measure the far field. Therefore a near-field testing facility is being planned. It is important, then, to know the relation between the near field and the far field. In particular,

the correlation between degradations of the near field and degradations of the far field must be known.

Both near fields and far fields may be calculated by the geometrical theory of diffraction (g.t.d.), as the satellite is large in terms of wavelengths. Although it is well known that g.t.d., when properly used, gives accurate results in the far field, less is known about the validity of g.t.d. in the near field. Therefore an investigation of g.t.d. near fields was carried out as part of a feasibility study for the METEOSAT near-field testing facility. This investigation is reported here.

Since the g.t.d. far field is a good approximation to the correct field, it is taken as reference and expanded into spherical harmonics.[2] The near field is then computed from the spherical expansion and the transformed field is compared to the g.t.d. near field.

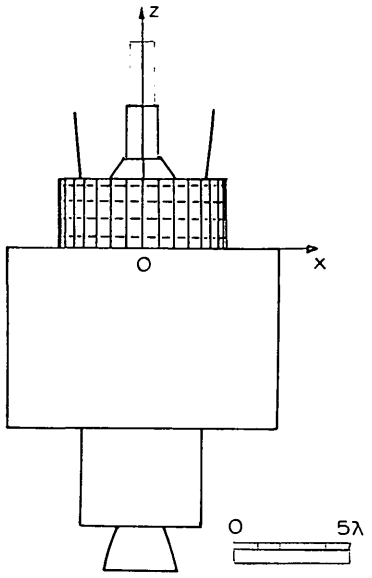

Fig. 1 *METEOSAT geometry and scale in wavelengths*

Calculation of g.t.d. fields: The near-field and the far-field calculations were carried out for four uniformly excited columns. The four elements in a column have an amplitude taper of $1:\sqrt{2}:\sqrt{2}:1$ and an interelement phase shift of 10° to remove an upward beam tilt caused by the satellite structure.

The g.t.d. far field and near field from the topmost element in a column are shown in Figs. 2*a* and *b*, respectively. The fields in front of the e.d.a. element are plotted as functions of the angle θ measured from the satellite axis. The distance from the origin (Fig. 1) to the near-field sphere is 11·2 wavelengths. The numbers on the curves indicate the rays included in the field calculations, as explained in Table 1. In the field calculations, the e.d.a. cylinder was assumed to be circular and uniform diffraction coefficients were used.[3] Creeping waves were omitted, so that the field close to, and inside, the shadow region of the e.d.a. cylinder is in error. In these directions, however, the pencil-beam antenna radiates only little power and the error may be neglected when the total e.d.a. field is considered.

The near-field and the far-field patterns in Fig. 2 differ significantly from each other because in the near field the relative phases of the ray contributions change rapidly and the distance attenuations differ from one ray to another. The width of the active part of the e.d.a. is about three wavelengths. This corresponds to a Rayleigh distance of 18 wavelengths. However, reflection and diffraction in the satellite makes a minimum far-field distance difficult to define. Owing to the influence of the satellite, the minimum far-field distance appears to be significantly larger than 18 wavelengths.

Transformation of g.t.d. far fields: Since the e.d.a. is a pencil-beam antenna, the far field was calculated only over the front hemisphere and was assumed to be zero over the back hemisphere. Based on this pattern, the spherical harmonics were computed, retaining 35 modes in the angle θ' measured from the array axis and a maximum of 32 modes in the angle ϕ' measured around the array axis. This is approximately the

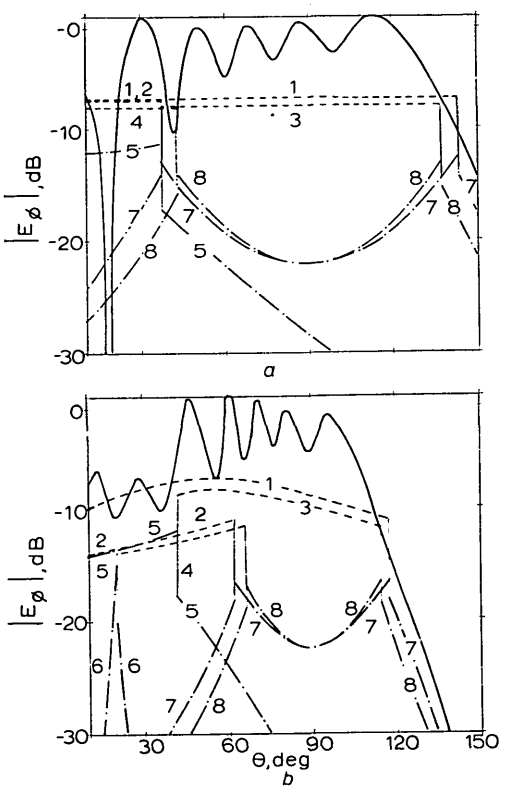

Fig. 2
G.T.D. far field (*a*) and near field (*b*) from topmost element in a column
——— total element field
– – – – geometric-optical rays
—·—· diffracted rays

Table 1

Ray	Description of ray
1	Direct
2	Reflected in main satellite body
3	Reflected in e.d.a. cylinder
4	Reflected in both e.d.a. cylinder and main satellite body
5	Diffracted in upper edge of e.d.a. cylinder
6	Reflected in main satellite body and diffracted in upper edge of e.d.a. cylinder
7	Diffracted in edge of main satellite body
8	Reflected in e.d.a. cylinder and diffracted in edge of main satellite body

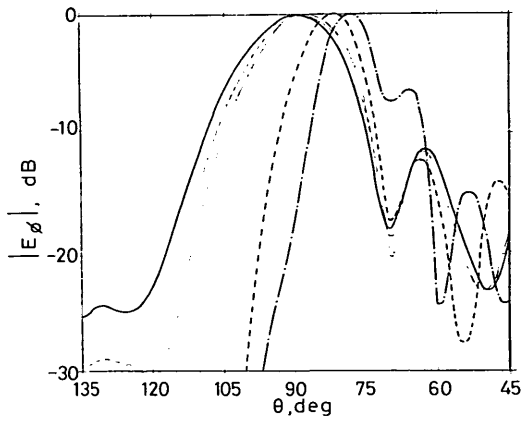

Fig. 3 *G.T.D. far field and transformed near fields*
——— g.t.d. far field
Transformed fields: – – – – 112 wavelengths away, —·—· 56 wavelengths away – – – – 11·2 wavelengths away and —·—· 6·7 wavelengths away

minimum number of modes required to transform the far field into the near field at the distances given below.[4] This number of modes allows the far field to be regenerated from the spherical expansion. The numerical problems which may arise in the transformation of the far field to the near field are avoided by the truncation of the spherical expansion.[4]

Fig. 3 shows the g.t.d. far field and the transformed fields at the distances 112, 56, 11·2 and 6·7 wavelengths away from the origin. The fields are normalised so that the maximum value corresponds to 0 dB. As the field points approach the satellite, the field maximum is shifted towards smaller values of θ.

The comparisons between the transformed fields and the g.t.d. near fields are shown in Figs. 4*a* and *b* for the distances of 11·2 and 6·7 wavelengths to the field points. The agreement is excellent for a distance of 11·2 wavelengths. Even for a distance of 6·7 wavelengths, where the nearest diffracting edge is only about 0·85 wavelengths away for $\theta = 90°$, the agreement is good. The small discrepancies in this case may be due to both the failure of g.t.d. near diffracting edges, where g.t.d. gives a singular field, and the increased importance of either inaccurately determined or neglected higher-order spherical modes in the near field.

It is therefore concluded that g.t.d. can be used to calculate the near field of the antenna system with an accuracy which is comparable to the accuracy obtained in the far field.

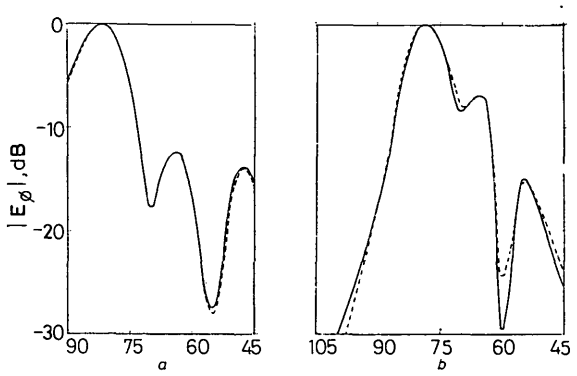

Fig. 4 *Comparisons between transformed fields and g.t.d. near fields*

——— g.t.d.
– – – – transformed field
(*a*) $r = 11·2$ wavelengths
(*b*) $r = 6·7$ wavelengths

Acknowledgments: This work was part of a study carried out for ESTEC under contract 2363/75/HP. The authors have pleasure in thanking N. E. Jensen, ESTEC, for his interest and encouragement.

N.CHR. ALBERTSEN
P. BALLING

TICRA A/S
Finlandsvej 6a
DK-2800 Lyngby
Denmark

28th August 1975

References

1 NICOLAI, C., and PALUMBO, B.: 'Studio e pro getto elettrico del sistema di antenna del satellite METEOSAT'. Conference proceedings of symposium on satellite and telecommunications, arranged by the Italian Electrical Association, Trieste, 1975
2 LUDWIG, A. C.: 'Near-field far-field transformations using spherical-wave expansions', *IEEE Trans.*, 1971, **AP-19**, pp. 214–220
3 KOUYOUMJIAN, R. G., and PATHAK, P. H.: 'A uniform geometrical theory of diffraction for an edge in a perfectly conducting surface', *Proc. Inst. Elec. Electron. Eng.*, 1974, **62**, pp. 1448–1461
4 LUDWIG, A. C.: 'Numerical check on the accuracy of spherical-wave expansions', *Electron. Lett.*, 1972, **8**, pp. 202–203

MILDLY SUBOPTIMAL DIGITAL FILTERS USING A HOST WINDOWING APPROACH

Indexing term: Digital filters

A digital-filter design technique is described which employs simple trigonometric windowing of a 'host' digital filter. In contrast to the usual windowing rationale which uses a truncated ideal impulse response, this approach uses an optimal (finite-length minimax) host impulse response. It is shown that optimal Hilbert-transform filters serve as suitable hosts for lowpass filters of even-length impulse response, and optimal differentiators can be used as hosts for odd-length impulse responses. The resulting windowed filters are no longer optimal, but yield approximation errors which are within a factor of two of optimal errors under most operating conditions.

Introduction: The well known windowing relationship

$$h_1(nT) = h_0(nT)w(nT) \quad . \quad . \quad . \quad . \quad . \quad . \quad . \quad . \quad (1)$$

gives the nth sample of a digital-filter's impulse response sequence, $\{h_1(nT)\}$, in terms of some underlying filter, having impulse response $\{h_0(nT)\}$, that is modified by the window sequence $\{w(nT)\}$. The normal method of filter design by windowing is to take $h_0(nT)$ as a direct ideal impulse-invariant version of the desired filters, e.g.

$$(\sin 2\pi f_c(n-k)T)/2\pi f_c(n-k)T$$

for a lowpass filter, and to select a $w(nT)$ that possesses attractive properties, such as a concentrated spectrum with low sidelobe levels, to impart an acceptably tapered weighting.

In this letter, we restrict attention to causal, finite-duration impulse-response (f.i.r.) filters, so $h_1(nT)$ and $w(nT)$, but often not $h_0(nT)$, vanish for values of the integer n outside the interval $[0, N-1]$. It has been observed that the straightforward window design method, although simple and easy to use, gives inferior error performance to procedures based on minimax error optimisation[1]. It should be noted in passing that, of course, the result of any filter design can be cast, retrospectively, as eqn. 1; hence an optimal f.i.r. filter can be viewed as the result of some custom-tailored optimal window being applied to $h_0(nT)$. Clearly, such an implicit window will be greatly sensitive to the specific constraints set out for $h_1(nT)$ and cannot be expected to be of general utility outside that particular context.

The purpose of this letter is to demonstrate that there is an appealing middle ground which permits construction of a wide range of nearly optimal f.i.r. filters still employing the simplicity of eqn. 1. The main point is that $h_0(nT)$ should be chosen to be an optimal f.i.r. 'host' filter; $w(nT)$ can be an elementary trigonometric window which explicitly uses the critical frequencies of interest.

Design technique: Our technique can be most easily seen where $h_0(nT)$ is taken to be an optimal f.i.r. digital Hilbert transformer. It has already been shown[2-4] that ideal lowpass filtering of a continuous time signal $x(t)$ can be expressed as

$$x_1(t) = \mathcal{H}[x(t)\cos 2\pi f_c t]\sin 2\pi f_c t - \mathcal{H}[x(t)\sin 2\pi f_c t]\cos 2\pi f_c t \quad (2)$$

where the indicated Hilbert transform operation is the convolution

$$\mathcal{H}[g(t)] = \frac{1}{\pi t} * g(t) \quad . \quad . \quad . \quad . \quad . \quad . \quad . \quad . \quad (3)$$

As explained in Reference 4, the 2-path quadrature modulation structure apparently dictated for digital implementation of eqn. 2 can be collapsed to the simple single-path formulation

$$x_1(kT) = x(kT) \circledast \{h_H'(nT)\sin 2\pi f_c \beta T\} \quad . \quad . \quad (4)$$

with $\circledast$ denoting discrete convolution and $\{h_H'(nT)\}$ being a sequence obtained by 'compacting', i.e. removing the alternate zeros in, an optimal odd-length f.i.r. digital Hilbert-transformer's impulse response; the quantity $\beta = n-(N-1)/2$ takes into account the time origin implicit in eqn. 2. These surviving N, where N is even, coefficients for $h_H'(nT)$ have been extracted from a Hilbert filter of the case-3 type (in the notation of Reference 1) having an impulse response $h_H(nT)$, of odd duration $2N-1$.

From eqn. 4, it can be seen that our technique for designing